Proceedings of IMECE2008
2008 ASME International Mechanical Engineering Congress and Exposition
October 31-November 6, 2008, Boston, Massachusetts, USA

IMECE2008-68190

EFFECT OF GEOMETRIC PARAMETERS OF SUPERHYDROPHOBIC SURFACE ON LIQUID SLIP

Choongyeop Lee
University of California, Los Angeles
Mechanical and Aerospace Engineering
Los Angeles, CA 90095, United States

Chang-Hwan Choi
Stevens Institute of Technology
Mechanical Engineering
Hoboken, NJ 07030, United States

Chang-Jin "CJ" Kim
University of California, Los Angeles
Mechanical and Aerospace Engineering
Los Angeles, CA 90095, United States

ABSTRACT

In this paper, we experimentally study how geometric parameters of textured hydrophobic surfaces affect a liquid slip, empowered by a custom-tuned microfabrication procedure that produces regular micro-patterns of posts and grates on an entire 4" wafer with a good size uniformity and no defect. A pitch of the patterns and a gas fraction of the structured surface are independently controlled, and the slip length over each type of patterns is measured using a rheometer system. On both grates and posts, the slip length increases linearly with a pitch but exponentially with a gas fraction. The trend of exponential increase by gas fraction appears more pronounced on posts than on grates. The defect-free surfaces allow the flows to maintain a de-wetted (Cassie) state at much higher pitches and gas fractions than previously possible, permitting flows with the maximum slip effect.

Keywords: superhydrophobic surface, liquid slip, wetting transition, drag reduction

INTRODUCTION

It has been well known that the roughness can modify the wettability between liquid and solid along with the surface chemistry [1,2]. In particular, the superhydrophobic surface, conventionally defined as the surface on which water forms over 150˚ of contact angle and invariably having a rough surface of hydrophobic material, has been widely investigated for its interesting properties such as water repellency and self cleaning [3-6].

Recently, another application of superhydrophobic surface was proposed; a large liquid slippage can be induced on superhydrophobic surface due to the composite interface consisting of liquid-solid and liquid-gas [7]. We can quantify the amount of liquid slippage using a slip length, which is defined as the virtual distance along the wall at which the liquid velocity extrapolates to zero. For example, tens of nanometers of slip length were measured on a hydrophobic surface [8]. It has been generally anticipated that a large liquid slippage will offer several advantages in various applications [9]: skin friction reduction [10], flow rate accretion [11,12], and the enhancement of interfacially driven transport such as electrophoresis and diffusion-osmosis [13]. Several experimental [14-20] and numerical [21-28] studies followed to determine the efficacy of superhydrophobic surfaces in increasing the slip length. In particular, recent experimental results demonstrated promising results, reporting hundreds of nanometers to tens of micrometers of slip length on superhydrophobic surfaces with irregular [14,15,17], semi-regular [18,19], and regular [16,20] patterns. However, it is still unclear how a slip length is affected by individual parameters such as a length scale and a gas fraction of the structured surface. For an optimal design of a liquid slipping surface, it is essential to understand the effect of individual parameter. In this study, we experimentally investigated how each of two main parameters – pitch and gas fraction – plays a role in the slip length using two different types of well-defined microstructures – post and grate. Based on our observation, we could optimize the surface parameters for maximum slip effect.

NOMENCLATURE

δ: slip length, L: pitch, ϕ_g: gas fraction

STABILITY OF SUPERHYDROPHOBIC SURFACE

For a superhydrophobic surface to be effective, it should stay in de-wetted state (Fig. 1). The condition for a de-wetted (fakir) state can be explained either using a thermodynamic energy minimization [29-31] or a force balance [32-34] between a liquid pressure and a surface tension. In the thermodynamic approach, it is considered that a wetted (Wenzel) and a de-wetted (Cassie) state are two distinct energy minimum points separated by the energy barrier. When the initial state is a de-wetted state, the state will be transitioned to the wetted state if the external pressure is large enough to overcome the energy barrier. In the force balance approach, the surface tension acting through the perimeter of structures is a restoring force against the liquid pressure. If the liquid pressure is larger than the total sum of surface tension, the superhydrophobic surface loses its stability and is transitioned to the wetted state. We used the latter approach [33] to find the condition for a de-wetted state in this study because of its simplicity.

For posts, the stability condition is given as

$$P_l \phi_g \le -4\gamma(1-\phi_g)\cos\theta / D \qquad (1)$$

while the stability condition for grates it is expressed as

$$P_l \phi_g \le -2\gamma \cos\theta / L \qquad (2)$$

Here, P_l is the liquid pressure, γ is the surface tension of a liquid (72×10^{-3} N/m for water at 25 °C), θ is the contact angle of a liquid on a flat surface (~120° for a water droplet on Teflon), and D is the top diameter of a post. We calculated the sustainable maximum gas fraction as a function of a pitch for a given pressure. The calculation results are summarized in Fig. 2, which shows what has been expected; the trend of a maximum gas fraction decreasing as a pitch and a liquid pressure increasing. More instructively, it clearly illustrates that a post and a grate have different behavior upon any changes in the pitch. For example, for a given pressure, grate patterns allow a high gas fraction at a small pitch, while post patterns are more advantageous in achieving a high gas fraction at a larger pitch.

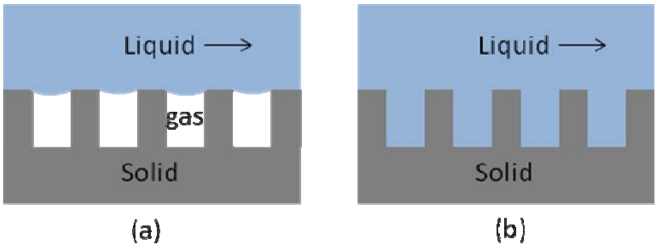

Figure 1 Two stable conditions. (a) De-wetted (fakir or Cassie) state, where a liquid flows over a surface, forming a composite interface of liquid-solid and liquid-gas. (b) Wetted (Wenzel) state, where a liquid completely wets surface.

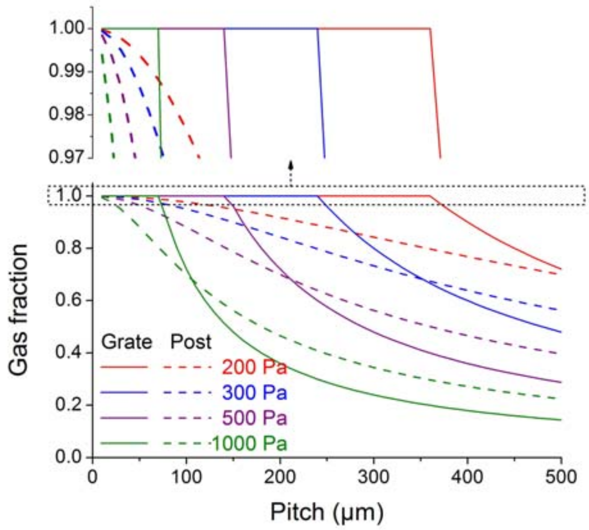

Figure 2 The stability condition for a de-wetted state. This condition is expressed as a maximum sustainable gas fraction as a function of a pitch for a given pressure. It is clearly shown that posts and grates exhibit a different functional behavior, although a general trend is similar.

For grates, the gas fraction can be as close as a unity for grates as far as the pitch is below the threshold for a given pressure (e.g. 250 μm of pitch for 300 Pa of water pressure). For posts, on the other hand, the gas fraction faces an upper limit regardless of the pitch. We designed superhydrophobic surfaces so that they could always meet the stability condition given in Fig. 2. The liquid pressure during the rheometry test was estimated to be 200-300 Pa.

SLIP MEASUREMENT

In this study, we utilized a commercial rheometer setup (AR 2000, TA Instruments) to measure a torque over the sample. The cone-and-plate geometry was used because it gives

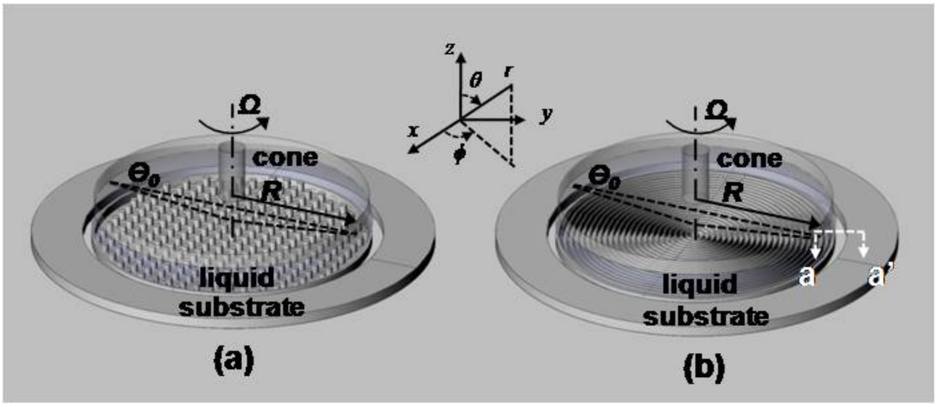

Figure 3 **The configuration of the rheometry setup for (a) posts and (b) grates.**

a constant shear rate over the whole test section. The cone has 60mm diameter and 2˚ cone angle, and 53 µm truncation was maintained between the cone and the sample. De-ionized (DI) water was used as a test liquid, and the temperature was controlled at 25 ± 0.1 ˚C by a Peltier plate during all the tests. For cone-and-plate geometry shown in Fig. 3, the shear stress is given by [18]

$$\frac{\partial \tau_{\theta\phi}}{\partial \theta} + 2\tau_{\theta\phi} \cot\theta = 0 \tag{3}$$

The boundary condition when there exists a slip velocity at the sample is given by

$$v_{\phi}(\frac{\pi}{2}, r) = v_s,\ v_{\phi}(\frac{\pi}{2} - \theta_0) = \Omega r \tag{4}$$

Here, v_s is the slip velocity at the sample, θ_0 is the cone angle and Ω is the angular velocity of the cone.

If we calculate the shear stress from the above equation and integrate the shear stress over the entire cone, we can obtain the following relationship between the torque and the slip length.

$$\begin{aligned} M &= \int_0^R 2\pi r^2 \tau_{\theta\phi} dr \\ &= \frac{2\pi}{3}\frac{\mu\Omega R^3}{\theta_0}(1 - \frac{3\delta}{2R\theta_0} + \frac{3\delta^2}{R^2\theta_0^{\ 2}}) - 2\pi\mu\Omega\frac{\delta^3}{\theta_0^{\ 4}}\ln(\frac{R\theta_0 + \delta}{\delta}) \end{aligned} \tag{5}$$

The torque was recorded in the shear rate ranging 90-130s^{-1} and was converted into the slip length using the above mathematical relationship. It is important to note that the above equation is the exact analytical form, which is extended from the approximated one used in [18]. When the slip length is larger than 50 µm, Taylor approximation used in [18] is not valid any more. In this study, where a large slip length is expected, we calculated the slip length by solving Eq. (5) numerically.

The errors generated from the rheometer test were analyzed for the same configuration before [18,35], and it was revealed that the dominant error resulted from the edge/end effects. The edge/end effects were mostly induced by the wettability on the surface and the amount of filling liquid. In particular, we tested samples with various wettabilities in this study, making a direct comparison among samples difficult. To minimize this error, we controlled the position and curvature of the liquid meniscus by implementing a ring of trench on every sample along the outer boundary of a test section as shown in Fig. 4. This trench anchors the contact line of the meniscus at its sharp top edge, so that the position of the meniscus is not affected by the surface wettability conditions. Then, we controlled the curvature of the meniscus by manually adjusting the liquid volume after the cone is in place. The shape of a free surface (meniscus) was then monitored by a high-speed camera during measurement (Fig. 4 (b)). Any discernible difference in the shape of meniscus among samples was not observed. From the images, we estimated that the deviation in the shearing radius was much less than 0.1 mm (or 7 µm in slip length), validating the accuracy of a rheometer system for the measurement of large slips.

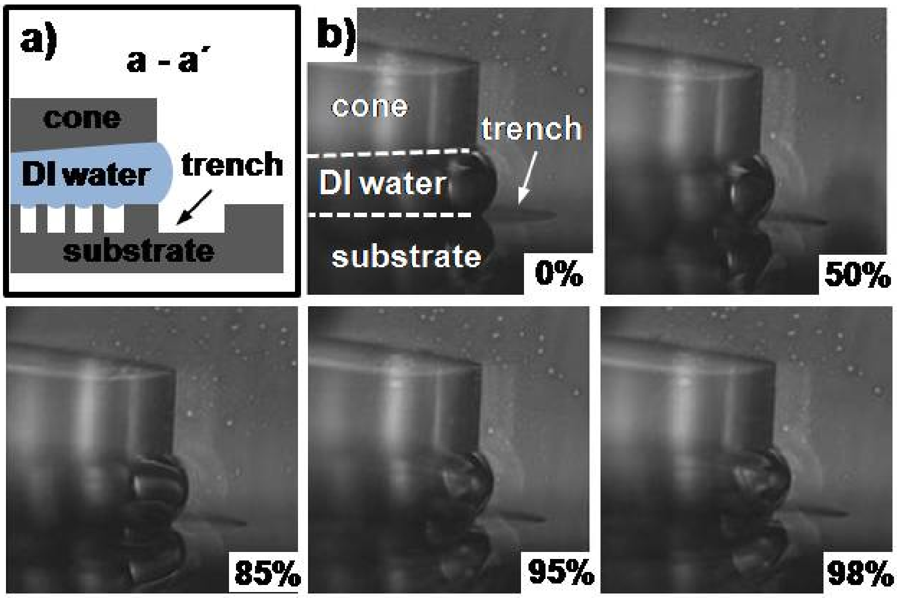

Figure 4 The error control by edge/end effects. (a) Cross section of a trench implemented along the outer boundary of a test section. See Fig. 3 for the location of the cross section. (b) Images of a liquid meniscus at the rim taken by a high speed camera for grates with 50 μm of a pitch and the following gas fractions: 0 (flat), 50%, 85%, 95% and 98%.

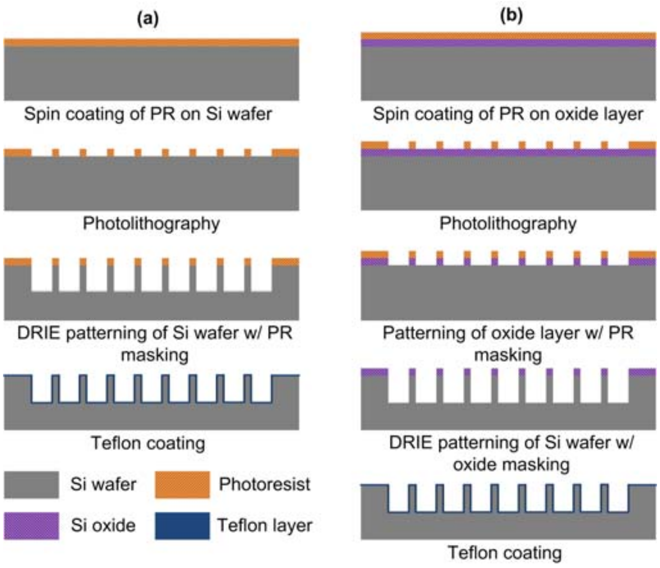

Figure 5 Process flow for sample fabrication. Most of samples were made using process (a). Only samples with grates over 150 μm pitch were made using process (b).

FABRICATION

For this study, well-defined microstructures (posts or grates) were fabricated on a 60 mm diameter circular area using conventional photolithographic technique. We decided to use microstructures instead of nanostructures since the dimension of structures was more suitable to control in microstructures. By using microstructures instead of nanostructures, the stability against wetting became a major issue. As a model structure, we tested posts and grates, since they facilitated the comparison with other numerical [22-24,27] and experimental [16,20] reports of a liquid slip on the same geometry. For grates, they were designed concentric so that they were parallel to the liquid flow as shown in Fig. 3(b). Although the conventional photolithographic steps were used to fabricate the structures, they needed a modification to make a surface free of defects. The defects on the test surface most likely acted as a wetting initiation point during the rheometer test. Once the wetting started, the wetting propagated everywhere for posts.

For grates, although the wetted area was confined within two adjacent grating lines, the resulting torque was still significantly larger than that without the wetting. Therefore, for all the tests, samples must be defect-free. In addition to the microscope inspection of surfaces during the sample preparation, each sample was visually checked after every flow test run to confirm that there was no wetted area on the surface. Only the data obtained with no wetting over the entire sample surface were accepted as valid ones. In order to engineer near-perfect samples in a Class 1000 cleanroom, we developed a customized photolithographic procedure involving several nonstandard measures. First, the 100 mm silicon wafer was thoroughly cleaned with Piranha solution (H_2SO_4:H_2O_2 = 4:1 in volume), rinsed with DI water, dried by a nitrogen gas, and dehydrated at 150˚C on a hot plate.

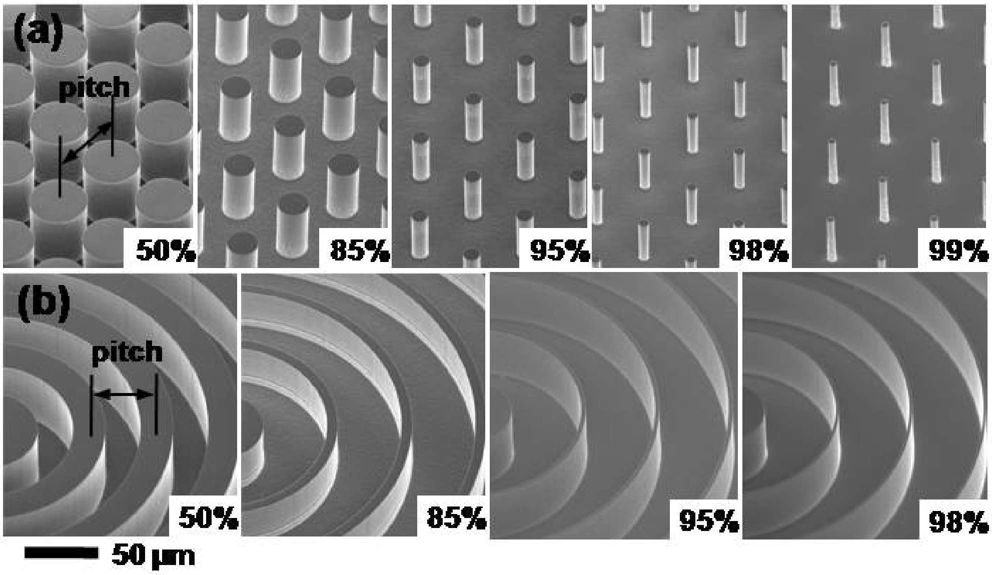

Figure 6 Scanning electron microscopy images of (a) posts and (b) grates with 50 µm of a pitch.

Then, the wafer was vapor-coated with hexamethyldisilazane (HMDS), which is the adhesion promoter between a photoresist (PR) and a wafer, by placing the wafer inside the glass beaker containing HMDS. Then, the surface of the wafer was inspected by ultraviolet (UV) illumination to ensure that there were no particles residing on the wafer. Once ensured, PR was spin-coated on the wafer. As a customized measure, the photoresist has been filtered through a membrane having 200 nm diameter holes. Using a particle counter, we confirmed that, during the spin-coating process, small particles were entrained onto the wafer by the inward air flow generated by the spinning. To address the particle issue, we isolated the spinner from the surroundings by covering it with a fixture of clean aluminum foil, which not only created a highly clean environment locally but also blocked the inward air flow from the surroundings. As a result, a near perfect PR coating was obtained. Then, PR was soft-baked at 100 ºC, exposed to UV light through a photomask on contact mode, and developed in 1:2 ratio AZ developer and DI water mixture. After the development, PR patterns on the test section (60 mm in diameter) were inspected under a microscope to ensure that there were no missing or broken patterns. After confirming that patterns were defect-free, the wafer was hard-baked at 120 ºC and ready for the etching step.

Most cases, we used deep reactive ion etcher (DRIE) to etch the silicon to the desired depth with the PR as a mask material. However, for samples over 150 µm of a pitch, we needed to etch the depth over 150 µm to make the depth the same as the pitch. In that case, due to the selectivity of PR to silicon in DRIE (1:75), silicon oxide (over two hundreds of the selectivity to silicon) was used as a mask layer instead. Silicon oxide (~500 nm) was thermally grown on silicon wafer and the aforementioned photolithography steps were done on the silicon oxide. Then, PR patterns were transferred into the silicon oxide by etching the silicon oxide with PR mask using the oxide etcher (STS Advanced Oxide Etcher). Then, silicon was etched to the desired depth (over 150 µm) by DRIE using silicon oxide as a mask material. The overall process flow is shown in Fig. 5. Figure 6 shows posts and grates with 50 µm of a pitch that were patterned on silicon wafer. Since the dimension on silicon wafer deviated from the dimension on the photomask during the above steps, we estimated the actual dimension by measuring the dimension at fifteen points along the radial direction using scanning electron microscopy. Most cases, we observed 200-500 nm variation from the target dimension on the photomask. After the fabrication, all the samples were treated to be hydrophobic by spin-coating a 2% Teflon AF® solution. Through SEM inspections in the top corner regions of the posts and grate, the coated Teflon was found negligibly thin (tens of nanometers at best). Therefore, we did not take into account the thickness of Teflon when we calculated the actual dimension of microstructures.

EXPERIMENTAL RESULTS

We investigated the effect of two parameters on a slip – a gas fraction and a pitch. To investigate the effect of a gas fraction on a slip, slip lengths were measured on samples with a fixed pitch of 50 µm but varying gas fractions – target gas fractions of 50, 85, 95, 98, 99, and 99.5% for posts and 50, 85, 95, and 98% for grates. For all the samples, the depth remained the same as the pitch (i.e., 50 µm). The slip lengths over the shear rate ranging 90-130 s^{-1} were listed in Fig. 7. Please note

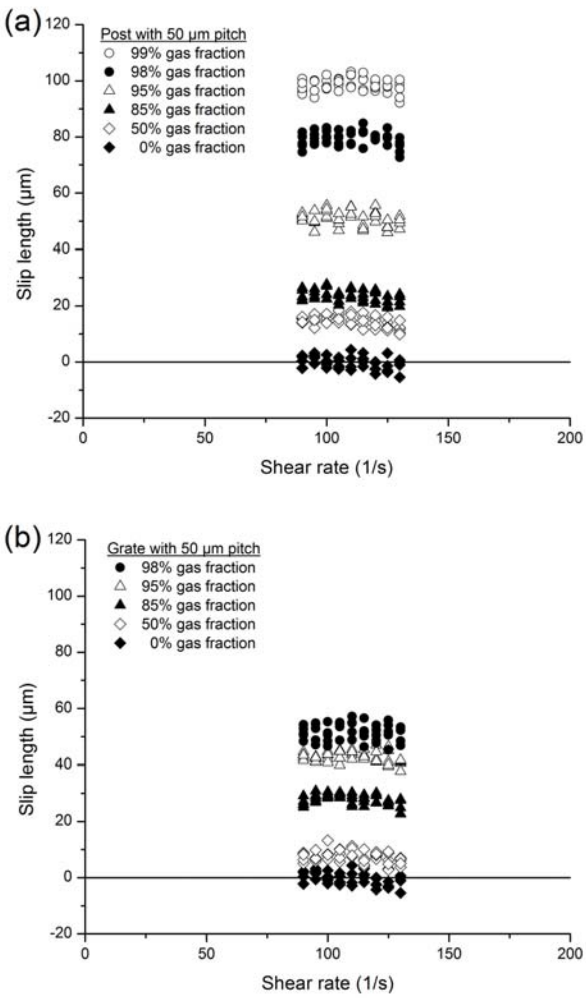

Figure 7 The effect of a gas fraction on a slip length for (a) posts and (b) grates with 50 µm pitch.

that the slip lengths stayed nearly constant regardless of the applied shear rate for both posts and grates.

All the slip lengths were collected, and the averages are shown in Fig. 8 along with the theoretical predictions available for posts [27] and grates [22]. The velocity field around grates was analytically solved in [36], and the analytical equation for slip length was derived in [22] is given as

$$\delta = \frac{L}{\pi}\ln(\sec(\phi_g \frac{\pi}{2})) \qquad (6)$$

For posts, the scaling law was used to develop the equation for a slip length at a high gas fraction limit [27]. This equation is given by

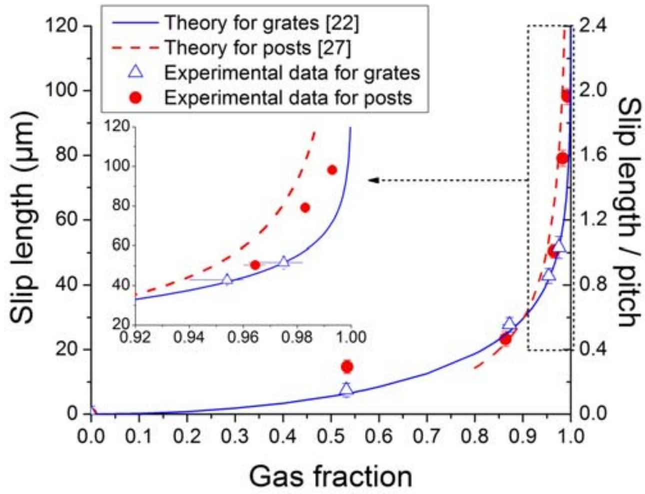

Figure 8 The comparison of measured slip length with the theory. The slip length increases more rapidly as a gas fraction approaches to a unity.

$$\delta = L(\frac{0.325}{\sqrt{1-\phi_g}} - 0.44) \qquad (7)$$

The coefficients in this equation were obtained through the numerical solutions for posts on a square lattice. On the other hand, the flow direction varies continuously with the underlying lattice in this study, since the rotational flow is imposed on the gird patterns of posts. Therefore, we can expect that there would be a discrepancy between the predicted slip length and the actual slip length resulting from inaccurate coefficients in Eq. (7). Still, it was considered that Eq. (7) could capture the qualitative characteristics of slip length at a high gas fraction.

Overall, the slip length exponentially increased as the gas fraction approached unity (100%), agreeing well with the theory [22,27]. On posts, the slip length increased more rapidly in the high gas fraction range than on grates in accord with the analytical scaling law [27] which predicts more rapid increase of slip length for posts. As stated before, the discrepancy of the experimental data from the theoretical value for posts can be considered due to the rotational flow pattern in the rheometer system. In comparison, the flow stays parallel to the grate patterns, and the discrepancy between the experimental and theoretical values was not significant (less than 3 µm). Please note that the maximum ratio of slip length to pitch reaches about two at 99% gas fraction for posts. From this one can clearly infer that the slip length is not always limited by its lateral length scale as suggested in [19]. Rather, the maximum

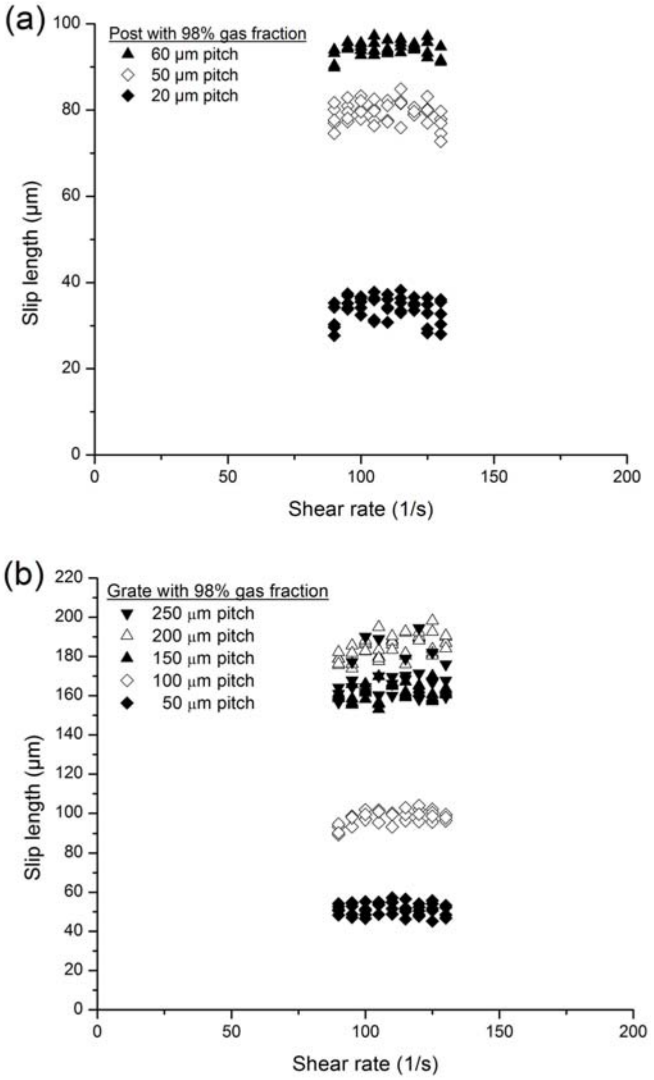

Figure 9 The effect of a pitch on slip length for (a) posts and (b) grates.

slip is constrained by the stability condition for a de-wetted state as discussed earlier. For our test where the liquid pressure ranges 200-300 Pa, the stability condition for posts in Fig. 2 predicts that the wetting transition occurs at the gas fraction of 99.4% when the pitch is 50 μm. The maximum gas fraction we could actually reach was 99.3% (or a target fraction of 99%), where the slip length of ~100 μm was achieved, which is twice as large as the pitch. At the gas fraction of 99.7% (or target fraction of 99.5%), the wetting transition was encountered as predicted by the theory. Our results becomes a clear indication that a slip length several times as large as a pitch might also be possible for high-gas fraction post structures if the pitch is reduced to enhance the transition stability, e.g., to be sub-micron as already demonstrated in [18]. For 1 μm-pitch posts, for example, a de-wetted state can be extended to a gas fraction higher than 99.99%, which will result in a theoretical slip length larger than 30 μm [27].

Secondly, we investigated the effect of pitch on a slip by measuring slip lengths on samples with the target gas fraction fixed at 98% but with varying pitches – 20, 50, and 60 μm for posts and 50, 100, 150, 200, and 250 μm for grates. The depth for each sample was maintained to be the same as the corresponding pitch. The slip lengths over the shear rate of 90-130 s^{-1} were plotted in Fig. 9. No dependency of slip length on a shear rate was observed in the applied shear rate range, so that the averaged slip lengths over this shear rate range were used for a comparison with a theory; both measured data and theoretical values are shown in Fig. 10. On both post and grate patterns, a slip increased linearly with a pitch. This result illustrates that, increasing a pitch in addition to increasing a gas fraction can be an effective method to enhance a slip effect despite the fact that there is an evident disparity in functional dependence (e.g., linear vs. exponential). However, we cannot increase the pitch indefinitely due to the condition for the wetting transition. For example, at the gas fraction of 98% and the pressure of 200-300 Pa, the maximum pitch for posts without the transition to wetting would be 60-100 μm according to the theory. On the other hand, at the same gas fraction and pressure, grates would allow larger pitches, up to 230-350 μm.

The maximum slip length in this study was obtained for grates with a pitch of 200 μm and was as large as 185 μm, a giant slip ten times larger than the previously reported maximum value [16,18]. At the pitch of 250 μm, no more increase in slip length was observed. Rather, the slip length at the pitch was lower than that at 200 μm. Also, the slip lengths for both pitches of 200 μm and 250 μm were lower than the theoretical values. We speculate that the liquid is not in purely Cassie state, but in the intermediate state between Cassie and

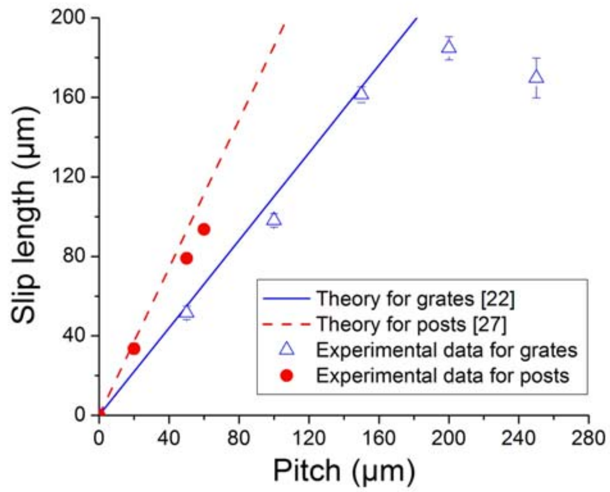

Figure 10 The comparison of measured slip lengths with a theory. The slip length increases linearly with a pitch for both posts and grates.

Wenzel state, although we could not confirm it by just looking for any visual changes on these two samples before and after the test.

Several studies [33,37] suggested that a liquid can stay in the intermediate state and the penetration depth depends on the liquid pressure and the surface parameters. Moreover, the close relationship between the location and shape of the liquid meniscus and the slip length was recently reported [28,38]. It was shown that the small change in the shape or location of a liquid meniscus can significantly reduce the slip length [28,38] and even lead to a negative slip length [38]. Therefore, we guess that the further increase in the slip length as a pitch became larger was not observed due to the increased penetration depth of the liquid meniscus resulting from the reduced stability to the wetting transition.

CONCLUSION

We have verified how geometric parameters of a superhydrophobic surface affect a slip. The summary of measured slip lengths in this study is listed in Table 1. A slip length was a linear function of pitch for both posts and grates. In accordance with a theory [22], a slip length was an exponential function of gas fraction for grates. For posts, more rapid increase of a slip length with a gas fraction was observed, as predicted by the equation derived by a scaling law [27]. By developing the microfabrication technique for a defect-free sample, we were able to successfully approach the theoretical thermodynamic limits for a de-wetting surface condition and achieved unprecedentedly large slips, up to 185 μm. The results confirmed that a high gas fraction and a large pitch within the thermodynamic boundary of Cassie state are two key surface parameters of superhydrophobic surfaces for a maximized slip effect. It should be noted that the giant slip observed in this report is larger than the length scale of many microfluidic systems and even approaches that of regular (macroscopic) systems. For example, the boundary layer thickness of a liquid flow over a macroscale object is in the order of millimetres [39] so that the maximized slip effect close to 200 μm will have significant effect even for the macroscale applications if the liquid pressure is small enough.

ACKNOWLEDGMENTS

This research has been funded by the National Science Foundation NIRT Grant 0103562 and California NanoSystems Institute (CNSI) Graduate Student Fellowship. The authors thank Professor Pirouz Kavehpour for help with the rheometer experiment.

Table 1 Summary of slip lengths measured for all the samples investigated in this study and the theoretical predictions for posts and longitudinal grates. A target diameter (or line width) refers to the feature dimension registered in a photomask, and a target gas fraction is calculated from the target diameter. Through several steps of a fabrication process, a feature size reduces from the target dimension. An actual diameter (or line width) refers to the feature size extracted from SEM images of the fabricated samples, and an actual gas fraction is calculated from the actual diameter.

Surface pattern	Pitch (μm)	Diameter (post) or line width (grate) (μm)		Gas fraction (%)		Slip length (μm)	
		Target	Actual	Target	Actual	Measured	Theory
Post	50	40.0	38.5	50	53.4	14.5	*N/A*
	50	22.0	20.8	85	86.4	23.5	22.1
	50	12.5	10.6	95	96.5	50.6	64.2
	50	8.0	7.3	98	98.3	79.3	102.6
	50	5.6	4.7	99	99.3	98.6	172.2
	50	4.0	3.3	99.5	99.7	wetting	274.7 if not wet
	20	3.2	3.2	98	98.0	33.6	37.2
	60	9.5	8.8	98	98.3	94.0	123.1
Grate	50	25.0	23.4	50	53.2	7.3	6.4
	50	7.5	6.4	85	87.2	27.7	25.6
	50	2.5	2.3	95	95.4	42.8	41.8
	50	1.0	1.3	98	97.5	51.6	51.5
	80	1.6	1.6	98	98.0	89.4	88.1
	100	2.0	1.5	98	98.4	106.5	117.3
	150	3.0	3.1	98	97.9	164.8	162.2
	200	4.0	4.0	98	98.0	187.8	220.3
	250	5.0	5.0	98	98.0	170	275.4

REFERENCES

[1] Wenzel, N. R., 1936, "Resistance of Solid Surfaces to Wetting by Water," Ind. Eng. Chem., **28**, pp. 988-994.
[2] Cassie, A.B.D. and Baxter, S., 1944, "Wettability on Porous Surfaces," Trans. Farad. Soc., **40**, pp. 546-551.
[3] Nakajima, A., Hashimoto, K., and Watanabe, T., 2001, "Recent Studies on Super-Hydrophobic Films," Monatshefte für Chemie, **132**, pp. 31-41.
[4] Blossey, R., 2003, "Self-Cleaning Surfaces - Virtual Realities," Nature Mater., **2**, pp. 301-306.
[5] Quéré, D., 2005, "Non-Sticking Drops," Rep. Prog. Phys., **68**, pp. 2495-2532.
[6] Roach, P., Shirtcliffe, N.J., and Newton, M.I., 2008, "Progress in Superhydrophobic Surface Development," Soft Matter, **4**, pp. 224-240.
[7] Kim, J., and Kim, C.-J., 2002 "Nanostructured Surfaces for Dramatic Reductions of Flow Resistance in Droplet-Based Microfluidics," *Proc. 15th IEEE International Conference on MEMS*, Las Vegas, United States, pp. 479-482.
[8] Choi, C.-H., Westin, J.A., and Breuer, K.S., 2003, "Apparent Slip Flows in Hydrophilic and Hydrophobic Microchannels," Phys. Fluids, **15**(10), pp. 2897-2902.
[9] Eijkel, J., 2007, "Liquid Slip in Micro- and Nanofluidics: Recent Research and Its Possible Implications," Lab Chip, **7**, pp. 299-301.
[10] Min, T., and Kim, J., 2004, "Effects of Hydrophobic Surface on Skin-Friction Drag," Phys. Fluids, **16**(7), PP. L55-L58.
[11] Majumder, M., Chopra, N., Andrews, R., and Hinds, B.J., 2005, "Enhanced Flow in Carbon Nanotubes," Nature, **483**, p. 44.
[12] Holt, J.K. et al., 2006, "Fast Mass Transport through Sub-2-Nanometer Carbon Nanotubes," Science, **312**, pp. 1034-1037.
[13] Ajdari, A., and Bocquet, L., 2006, "Giant Amplification of Interfacially Driven Transport by Hydrodynamic Slip: Diffusio-Osmosis and Beyond," Phys. Rev. Lett., **96**, 186102.
[14] Watanabe, K., and Udagawa, H., 1999, "Drag Reduction of Newtonian Fluid in a Circular Pipe with a Highly Water-Repellent Wall," J. Fluid Mech., **381**, pp. 225-238.
[15] Balasubramanian, A.K., Miller, A.C., and Rediniotis, O.K., 2003, "Microstructured Hydrophobic Skin for Hydrodynamic Drag Reduction," AIAA J., **42**(2), pp. 411-414.
[16] Ou, J., Perot, B., and Rothstein, J.P., 2004, "Laminar Drag Reduction in Microchannels Using Ultrahydrophobic Surfaces," Phys. Fluids, **16**(12), pp. 4635-4643.
[17] Gogte, S. et al., 2005, "Effective Slip on Textured Superhydrophobic Surfaces," Phys. Fluids, **17**, 051701.
[18] Choi, C.-H., and Kim, C.-J., 2006, "Large Slip of Aqueous Liquid Flow over a Nanoengineered Superhydrophobic Surface," Phys. Rev. Lett., **96**, 066001.
[19] Joseph, P., et al., 2006, "Slippage of Water Past Superhydrophobic Carbon Nanotube Forests in Microchannels," Phys. Rev. Lett., **97**, 156104.
[20] Choi, C.-H., et al., 2006, "Effective Slip and Friction Reduction in Nanograted Superhydrophobic Microchannels," Phys. Fluids, **18**, 087105.
[21] Cottin-Bizonne, C., Barrat, J.-L., Bocquet, L., and Charlaix, E., 2003, "Low-Friction Flows of Liquid at Nanopatterned Interfaces," Nature Mater., **2**, pp. 237-240.
[22] E. Lauga, and Stone, H.A., 2003, "Effetive Slip in Pressure-Driven Stokes Flow," J. Fluid Mech., **489**, pp. 55-77.
[23] Cottin-Bizonne, C. et al., 2004, "Dynamics of Simple Liquids at Heterogeneous Surfaces: Molecular-Dynamics Simulations and Hydrodynamic Description," Eur. Phys. J. E, **15**, pp. 427-438.
[24] Priezjev, N.V., Darhuber, A.A., and Troian, S.M., 2005, "Slip Behavior in Liquid Films on Surfaces of Patterned Wettability: Comparision between Continuum and Molecular Dynamics Simulations," Phys. Rev. E, **71**, 041608.
[25] Sbragaglia, M., et al., 2006, "Surface Roughness-Hydrophobicity Coupling in Microchannel and Nanochannel Flows," Phys. Rev. Lett., **97**, 204503.
[26] Sbragaglia, M., and Prosperetti, A., 2007, "Effective Velocity Boundary Condition at a Mixed Slip Surface," J. Fluid Mech., **578**, pp. 435-451.
[27] Ybert, C., et al., 2007, "Achieving Large Slip with Superhydrophobic Surfaces: Scaling Laws for Generic Geometries," Phys. Fluids, **19**, 123601.
[28] Biben, T., and Joly, L., 2008, "Wetting on Nanorough Surfaces," Phys. Rev. Lett., **100**, 186103.
[29] Patankar, N.A., 2003, "On the Modeling of Hydrophobic Contact Angle on Rough Surfaces," Langmuir, **19**, pp. 1249-1253.
[30] Ishino, C., Okumura, K., and Quéré, D., 2004, "Wetting Transitions on Rough Surfaces," Europhys. Lett., **68**(3), pp. 419-425.
[31] Barbieri, L., Wagner, E., and Hoffmann, P., 2007, "Water Wetting Transition Parameters of Perfluorinated Substrates with Periodically Distributed Flat-Top Microscale Obstacles," Langmuir, 23, pp. 1723-1734.
[32] Extrand, C.W., 2004, "Criteria for Ultrahydrophobic Surfaces," Langmuir, **20**, pp. 5013-5018.
[33] Zheng, Q.-S., Yu, Y., and Zhao, Z.-H., 2005, "Effects of Hydraulic Pressure on the Stability and Transition of Wetting Modes of Superhydrophobic Surfaces," Langmuir, **21**, pp. 12207-12212.
[34] Extrand, C.W., 2006, "Designing for Optimum Liquid Repellency," Langmuir, **22**, pp. 1711-1714.
[35] Choi, C.-H., and Kim, C.-J., 2006, "Reply to Comments on 'Large Slip of Aqueous Liquid Flow over a Nanoengineered Superhydrophobic Surface'," Phys. Rev. Lett., **97**, 109601.
[36] Philip, J.R., 1972, "Flows Satisfying Mixed No-Slip and No-Shear Conditions," ZAMP, **23**, pp. 353-372.
[37] Moulinet, S., and Bartolo, D., 2007, "Life and Death of a Falkir Droplet: Impalement Transitions on Superhydrophobic Surfaces," Eur. Phys. J. E, **24**, pp. 251-260.

[38] Steinberger, A., Cottin-Bizonne, C., Kleimann, P., and Charlaix, E., 2007, “High Friction on a Bubble Mattress,” Nature Mater., **6**, pp. 665-668.
[39] White, F.M., 1994, Fluid Mechanics, McGraw-Hill, 1994, Chap. 7.